Journal of Nuclear Materials 534 (2020) 152151

Contents lists available at ScienceDirect

Journal of Nuclear Materials

journal homepage: www.elsevier.com/locate/jnucmat

Effect of He content on microstructure, mechanical properties and He thermal desorption behavior of W film fabricated by RF magnetron sputtering

Le Wang [a, b], Qunbo Fan [a, b, *], Ting Hao [c], Duoduo Wang [a, b], Xinjie Zhu [a, b], Haichao Gong [a, b], Xin Liu [b]

[a] Beijing Institute of Technology Chongqing Innovation Center, Chongqing, 401135, China
[b] National Key Laboratory of Science and Technology on Materials Under Shock and Impact, School of Materials Science and Engineering, Beijing Institute of Technology, Beijing, 100081, China
[c] Key Laboratory of Materials Physics, Institute of Solid State Physics, Chinese Academy of Sciences, Hefei, 230031, China

ARTICLE INFO

Article history:
Received 4 February 2020
Received in revised form
1 April 2020
Accepted 3 April 2020
Available online 11 April 2020

Keywords:
Magnetron sputtering
He-charged W films
Microstructure
Thermal desorption
He bubbles
Hardness

ABSTRACT

In order to study the effect of He content on microstructure, mechanical properties and He thermal desorption behavior of W film, He-charged W films on Si substrates were fabricated by a radio frequency (RF) magnetron sputtering device in different He/Ar mixture gases. The deposited W films had a typical columnar structure, and the grain size of W films decreased as He/Ar ratio increased by means of the observation of scanning electron microscopy (SEM). X-ray diffraction (XRD) analysis confirmed that W films had a typical bcc structure, and the introduced He atoms can refine grain size and increase the lattice strain. TEM analysis showed that large numbers of He bubbles can be formed in W films, as well as the size and density of these He bubbles increased with the increase of the He/Ar ratio. The shape of He bubbles trapped by different sites also had some differences. Thermal desorption spectra (TDS) revealed that He content increased with He/Ar ratio increasing and different types of He atoms could be introduced into W films. The hardness value measured by nanoindentation tests increased with He/Ar ratio increasing, which demonstrated that nano-sized He bubbles could strengthen W films.

1. Introduction

Tungsten (W) has a high melting point, low sputtering yield, good mechanical properties, and low tritium retention so that it has been considered as one of the most important structural materials of the plasma-facing component (PFC) in the divertor and baffle regions of ITER and DEMO [1–5]. Plasma facing materials (PFMs) not only are exposed to steady-state and transient heat load up to ~20 MW/m^2 but also suffer the radiation of 14 MeV neutrons from the reaction D+T→ n (14.06 MeV)+α (3.52 MeV) [6,7]. The α particles, i.e., He atoms, can be easily accumulated in PFMs, e.g., W. These accumulated He atoms are prone to be trapped by various defects because of their insolubility and high mobility in metals, leading to the formation of He-vacancy aggregations [8] and He bubbles [9]. With the increase of accumulation amount, He atoms trapped by defects have a strong tendency to precipitate into larger bubbles [5], which will consequently cause performance deterioration of structural materials, such as swelling, surface blistering, crack, and flaking [10–12]. Accordingly, the influence of He on fusion materials is a critical issue.

On the other hand, nanocrystalline structural materials have the unique properties of irradiation resistance, with the high density of dislocation and the large volume fraction of grain boundaries which can act as an important sink for radiation-induced point defects [13–16]. Generally, W nanocrystalline films produced by magnetron sputtering have a columnar grain structure. Qin et al. [17] reported that the W columnar grain deposited by magnetron sputtering can provide the nanochannel structure to increase the releasing of He atoms and thus to minimize the He nucleation. The results demonstrate that W film with a columnar grain structure have better radiation resistance. Therefore, a detailed investigation

* Corresponding author. National Key Laboratory of Science and Technology on Materials Under Shock and Impact, School of Materials Science and Engineering, Beijing Institute of Technology, Beijing, 100081, China.
E-mail address: fanqunbo@bit.edu.cn (Q. Fan).

https://doi.org/10.1016/j.jnucmat.2020.152151
0022-3115/

about He effects on properties of nanocrystalline W films is very necessary.

To date, there are a few methods which can introduce He atoms into investigated samples. For example, neutron irradiation was performed on W bulk materials by Takashi Tanno et al. [18] and Akira Hasegawa et al. [19]. Some researchers also adopted the method of radioactive decay of tritium in metal tritides to study He behavior of metal tritides [20,21]. In addition, He ion implantation as an important way was developed to investigate He effects on the W materials [22–26]. However, it should be noted that neutron irradiation can cause a large amount of neutron-induced damages, and He produced may be immediately captured by the concurrent damage, which appends the complexity of the He behavior investigation. Also, the radioactive decay of tritium needs a long time and dangerous operating condition with tritium, for tritium is radioactive with a half-life of 12.3 years. Moreover, for He ion implantation, low energy (from several tens to several hundreds of eV) He implantation can only introduce these helium atoms at rather shallow depth below the surface. For He implantation with high energy, it is very hard to obtain uniform distribution in the depth direction. At the same time, it will also produce displacement damages and influence He diffusion, He agglomeration and bubble nucleation, as well as He distribution in metals is not uniform. Therefore, the above two methods of introducing He atoms into materials aren't the most suitable way to study He effect on W material.

Recently, magnetron sputtering as a new method which can introduce He atoms into the growing films has been developed. D.M. Mattox et al. [27] were first to use this method of magnetron sputtering to prepare He-charged gold films in pure He gas. However, for He gas, it is difficult to obtain stable glow. Thus, some scientists have prepared a variety of He-charged metal films by magnetron sputtering in a He/Ar mixed atmosphere. For example, Ti films with high He concentration by Zheng et al. [28] and Shi et al. [29], He-charged Al films by Jia et al. [30] and He-charged FeCrNi-based films by Song et al. [31]. During the sputtering process, the sputtering yield of He atom to metal was much smaller than that of Ar atom, but the backscattering probability of He atom to the heavy nuclei was greatly larger than that of Ar atom [32]. Therefore, during the He-charged film deposition, the main effect of Ar atoms is to increase the deposition speed and the introduced Ar concentration is almost negligible.

Compared to other approaches to introduce He into materials, magnetron sputtering proposed by us is an effective, safe and economical technique. The concentration of helium could be regulated and controlled by adjusting He/Ar ratio. It also makes the introduction of different He contents easier than other methods. Meanwhile, for He-charged tungsten films prepared by magnetron sputtering, no irradiation damage was introduced into the metal matrix, which can avoid the influences of irradiation-induced artificial defects when behavior and evolution of helium in tungsten film are studied.

In our previous experiment, we had fabricated He-charged W films by means of RF magnetron sputtering in a mixed gas of He/Ar = 1 to study the evolution of He bubbles and He desorption behavior in W films during annealing [33]. However, the effect of He content on He-charged tungsten film wasn't investigated before. In addition, in nuclear materials research, He content is one of the most important factors influencing the mechanical properties of nuclear materials and He behavior. Therefore, in the present study, in order to study the effects of He concentration on the microstructure and thermal desorption behavior of W films, we prepared W film with different He concentrations by RF magnetron sputtering in mixed gases with various He/Ar ratios (He/Ar = 0, 1, 2 and 3, respectively). The results presented in this work can contribute to better understanding He effects on microstructure and nanohardness of W films, He desorption behavior and the distribution of He bubbles in W film.

2. Experimental details

In the present work, W films with different helium concentrations were prepared by RF magnetron sputtering in the mixed atmospheres with different He/Ar ratios. W disk (purity 99.95% and 60 mm in diameter) was employed as the target. The distance between the target and the substrate was 5 cm. The substrates on which the films were deposited are p-type Si single crystals with a (111) preferred orientation. Before the experiment, the Si discs were boiled in a solution (HCl: H_2O_2: H_2O = 1:1:6) at 70–90 °C for 15min and further ultrasonically rinsed in a mixed solution of ethanol and acetone for 10min, blow-dried. At last, the Si discs were cleaned by deionized water for several minutes and blow-dried. During the experiment, the substrates were not heated, but the actual temperature (about 70 °C) was higher than room temperature (RT) as the collision of the W atoms and the substrates each other. Prior to depositing He-charged W films, the base pressure was evacuated to a pressure value of below 8.0×10^{-4} Pa by a turbo molecular pump. The working gases were a mixture of 99.99% purity Ar and 99.99% purity He. The Ar particle pressure was confined at about 0.6 Pa, and the sputtering power was controlled at 80 W. W films with different He concentrations were obtained by adjusting He/Ar ratio at 0, 1:1, 2:1, 3:1. In this experiment, the flux of Ar was 10.0 sccm and the flux of He was varied to get samples containing different He concentrations.

The surface and cross-sectional morphology of the prepared films were analyzed by field emission scanning electron microscopy (FESEM, Oxford INCA). The accelerating voltages for SEM are 5 keV.

The evolution of the crystal structure W films deposited on the Si substrate with different amounts of He was characterized by an X-ray diffractometer (XRD, A Philips X'Pert PRO). This diffractometer equipped with a Cu Kα radiation (wavelength: 0.15418 nm) was used in a 2θ mode, 2θ varying from 30° to 90° with 0.06°/step.

The size and distribution of He bubbles in W films can be observed by TEM. Conventional bright-field and high-resolution image observations were performed in a CM 2000 TEM with field emission gun. Cross-sectional TEM samples were prepared by a special method combining the methods of mechanical thinning with Ar ion milling. Each TEM sample was a lamella (3 mm in diameter), which consisted of two identical sample slices glued face to face (3 mm × 2 mm) and a Mo support ring. The thickness of the TEM observation area was about 50 nm. To confirm the existence of He bubbles precisely, the observation of He bubbles was conducted at an under-focus condition (~800 nm) so that these bubbles appeared as white disks surrounded by dark fringes. The average size of He bubbles can be obtained by calculating the diameter of more than 300 He bubbles.

Thermal desorption spectra (TDS) of He-charged W films were obtained in a thermal desorption spectrometer with a vacuum of about 2×10^{-10} Torr. The films deposited on Si substrates are heated in a quartz tube by a program-controlled high-temperature furnace in the air. A linear temperature ramp of 1 °C/s is adopted from room temperature up to 1000 °C. He release rate changing over time was recorded by a quadrupole mass spectrometer (QMS). Through measuring the variation of He atom releasing rate with temperature, the kinetics of helium desorption from He-charged W films can be confirmed.

Nanohardness of W films with various He concentration was characterized by a nanoindenter (Nanoindenter G200, Agilent Technologies) with a diamond Berkovich (three-sided pyramidal)

tip and an optical microscope. During the experiments, the displacement resolution of 0.02 nm and load resolution of 50 nN were conducted, respectively. The hardness (H)—depth (h) profile was obtained in a continuous stiffness measurement (CSM) model. The maximum indentation depth was about 1 μm, which was less than the thickness of the prepared W films. Ten indents were conducted on each sample, and the average hardness was determined through averaging the ten indention values.

3. Results and discussion

3.1. The morphology and crystal structure of He-charged W films

Fig. 1 shows the effect of He atoms on the surface morphology of W films. As shown in Fig. 1, the structure of both pure W films and He-charged W films are very compacted. For W film deposited by magnetron sputtering, there may be some nano-scale grains in films, which can be hardly detected by SEM. Moreover, not all grain boundaries in the deposited film can be easily shown in SEM images, which may cause some the measurement errors. Therefore, the SEM images can't assess accurately the average grain size. Nevertheless, the SEM images of surface morphology still can indicate roughly that the grain size becomes smaller with increasing He/Ar ratio. The trend of the change of grain size obtained from the surface SEM images corresponds to the following result of grain size calculated by the XRD peak profile analysis.

To observe the cross-section morphology of W films on the Si substrate, the cross-section morphology SEM images are shown in Fig. 2. It can be easily seen that all W films prepared at different He/Ar ratios have the typical and dense columnar crystalline structure and the thickness of the films is about 5 μm. The grain size is so fine that we can hardly confirm the actual grain size by means of SEM images.

To obtain the grain size and crystalline structure of W films, X-ray diffraction (XRD) technique was used. Fig. 3 shows the XRD spectra of the W films on the Si substrates prepared under different He/Ar ratios. The four diffraction peaks in the XRD patterns corresponded to the crystalline faces of (110), (200), (211) and (220). As shown in Fig. 3, the peak width became broader gradually with increasing of He/Ar ratios. A similar phenomenon was also observed in He-charged Al films [31]. For the reason of the increase of the peak width, it may be caused by the introduced He atoms during the deposition process. These He atoms not only refine the grain size but also increase the strain. X-ray diffraction peak profile analysis can be used to determine the mean grain size and strain. Based on the above analysis, the line broadening of XRD arises mainly due to three factors: the instrumental influence, the strain broadening and the effects based on size effect. Therefore, before estimating the grain size and strain, it is necessary to correct the instrumental effect. The instrumental corrected broadening β_{hkl} corresponding to the diffraction peak of W was estimated using the relation [34]:

$$\beta_{hkl} = \left[(\beta_{hkl})^2_{measured} - \beta^2_{instrumental}\right]^{\frac{1}{2}} \quad (1)$$

Assuming that the W films grain size and strain contributions to line broadening are independent to each other and both have a Cauchy-like profile, Williamson and Hall developed a method known as the Williamson-Hall plot (WHP) [35]:

$$\beta_{hkl}cos\theta = \left\{\frac{k\lambda}{D}\right\} + 4sin\theta\varepsilon \quad (2)$$

where D is grain size, θ is Bragg reflection angle, K is constant also known as crystallite shape factor taken as 0.94, λ is the wavelength of the incident beam: 0.15418 nm, β_{hkl} is the instrumental corrected broadening, ε is lattice strain.

According to the Williamson-Hall plot, $\beta_{hkl}cos\theta$ is plotted with respect to $4sin\theta$ for the corresponding peak of W films. Strain and grain size can be calculated from the slope and y-intercept of the fitted line respectively. By the Williamson-Hall plot, the calculated grain size and lattice strain of W films containing different helium concentrations have been shown in the following Fig. 4.

From the result of Fig. 4, it is clear that crystallite size decreases and strain increased with the increase of He/Ar ratio. When He/Ar = 0, the grain size of pure W films is 113 nm. When He/Ar = 1,

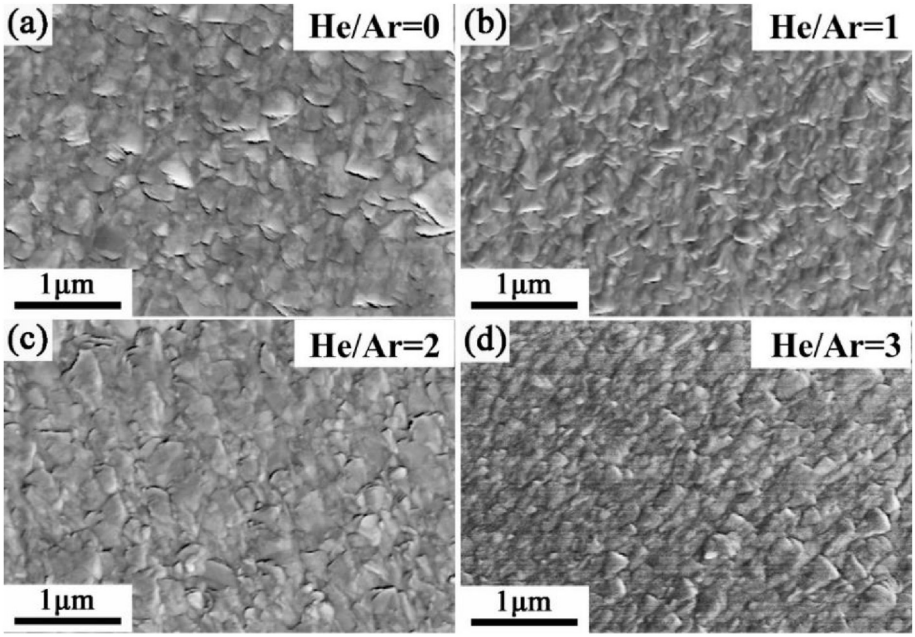

Fig. 1. The surface SEM images of W films deposited on the Si substrate at RT under the different He/Ar ratios: (a) 0; (b) 1; (c) 2; (d) 3.

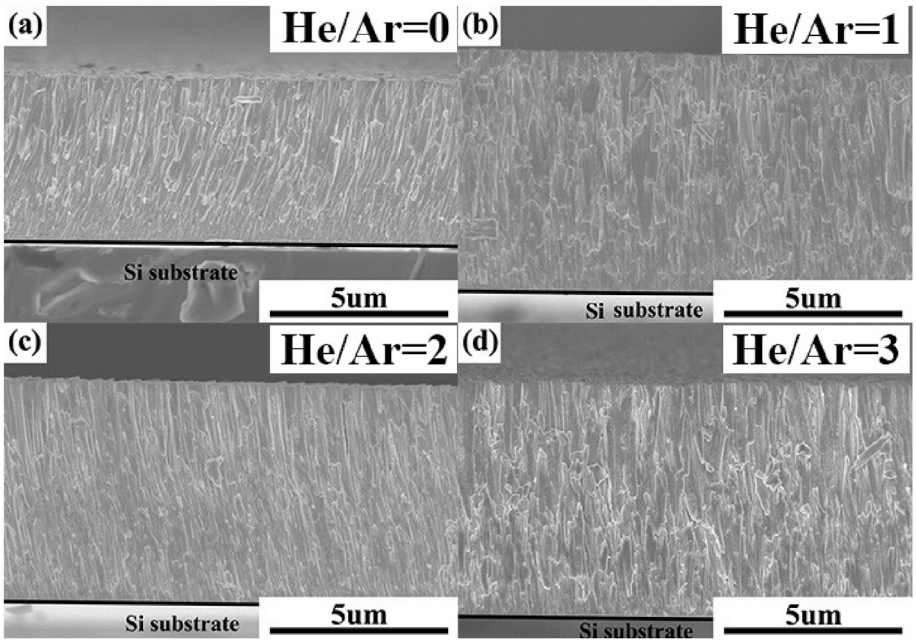

Fig. 2. Cross-sectional morphology of W films prepared under different He/Ar ratios: (a) He/Ar = 0; (b) He/Ar = 1; (c) He/Ar = 2; (d) He/Ar = 3.

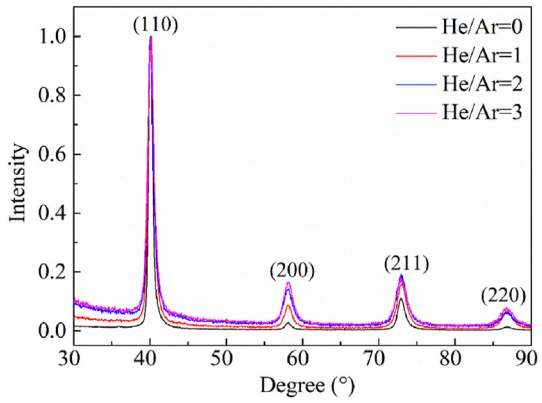

Fig. 3. XRD patterns of W films fabricated under different He/Ar ratios at RT on Si substrates.

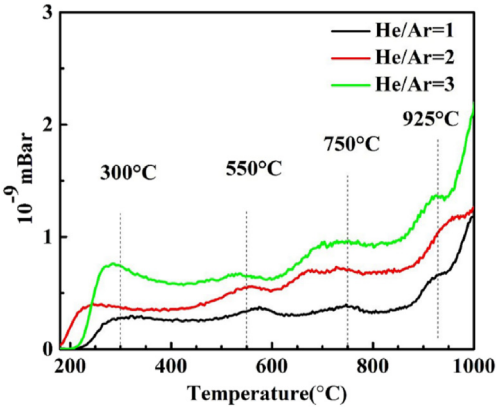

Fig. 5. Thermal desorption spectra of He in W films fabricated on Si substrates at room temperature (RT) under three He/Ar ratios of 1:1, 2:1 and 3:1.

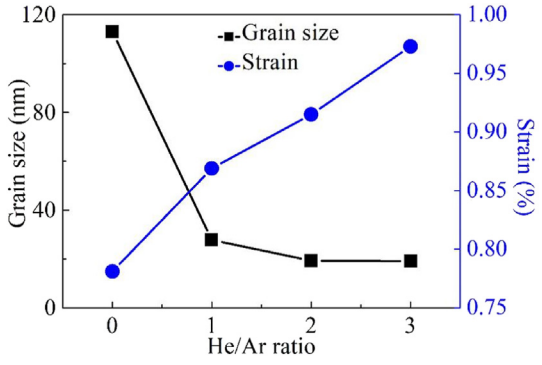

Fig. 4. The crystallite size and strain of W films prepared under different He/Ar ratios at RT on Si substrates.

the grain size is 27.8 nm. This demonstrates that the introduction of He atoms can refine distinctly grain size from He/Ar = 0 to He/Ar = 1. However, the gain size is almost constant when He/Ar ratio was from 2 to 3. It indicates that refinement of grain size reached a saturation level at the higher He/Ar ratio, and further refinement became quite difficult. The strain always increased with He/Ar ratio increased, which was mainly the result of self-interstitial formation associated with bubbles formation resulting in strain fields.

3.2. TDS analysis

It is well known that we can obtain the existing form of He atoms from different trapping sites in materials by mean of the TDS spectra. The higher desorption peak temperatures in TDS spectra correspond to the stronger binding energy between He atoms and defects, which also means that the release of He atoms from the corresponding site for trapping will become more difficult. Fig. 5 shows the TDS spectra of He in W films fabricated on Si substrates in mixed gases with different He/Ar ratios (1:1, 2:1, 3:1) at RT. Each profile consists of some broad and overlapping peaks, which is the superposition of release of He atoms located in different trapping sites. From the TDS spectra, it is clear to see that,

Table 1
He desorption peak temperature of He-charged W films prepared by magnetron sputtering under different He/Ar ratios.

He/Ar ratio	Peak temperature (°C)			
1	300	580	750	925
2	250	550	710	950
3	280	525	740	925

the total release of He from He-charged W films increases from He/Ar = 1 to He/Ar = 3, which implies that higher He/Ar ratio can result in increased He atoms trapped into W films. For the three desorption profiles in Fig. 5, these peaks all located around similar temperature regions that include about 300 °C, 550 °C, 750 °C, and 925 °C. Meanwhile, we can find that a large amount of He atoms would be released at more than 1000 °C, but the peak can't absolutely appear because of the limit of the instrument. The actual desorption peak temperature of W films is shown in the following Table 1.

As Fig. 5 and Table 1 shown, the corresponding peak temperature in the three TDS profiles is not exactly the same. However, the effect of He/Ar ratio on desorption peak temperature has no obvious regularity. Nevertheless, the above results also suggest that the existing form of He atoms introduced into W films prepared by magnetron sputtering in mixed gases with different He/Ar ratios has some slight differences. This can be explained that the number of He atoms trapped by the identical defect may be different under various He/Ar ratios, because the difference of the number of He atoms can change the desorption energy of He. The detailed analysis is discussed in the follows.

To date, many researchers had investigated the TDS spectra of He in W samples. Especially in our previous work, we had examined He desorption behaviors of He-charged W film annealed at different temperatures and found that He desorption behaviors of as-deposited He-charged W film prepared by magnetron sputtering was similar to that in W bulk irradiated by low energy He ions [33]. It was reported that there were also four desorption peaks located at about 300 °C, 625 °C, 700 °C and 850 °C for as-deposited He-charged W films. This phenomenon was approximately in agreement with the result in Table 1. Based on the conclusion of reference [33], we can obtain the desorption mechanism of He atoms trapped by various sites. For these peaks around 300 °C, they may be the results of the release of He clusters at interstitial sites, since He atoms were trapped weakly by interstitial sites. A similar phenomenon was also observed in the case of nanochannel W film irradiated by 40 keV He^+ ion with a fluence of 3×10^{17} ions cm^{-2} [36]. And He releasing peaks at about 550 °C, 750 °C, and 925 °C should be caused by He-vacancy(V) complexes (including He_n-V and He_nV_m). In terms of He_n-V and He_nV_m, the binding energy of He atoms to He-vacancy complexes decreases with the increase of n and increases with the increase of m. In other words, the binding energy of He atoms to He-vacancy complexes decreases with the increase of He/V ratio [37]. Therefore, for the peaks at about 550 °C, it was attributed to the release of He atoms from He-vacancy complexes with higher He/V ratio, and for the peaks at 750 °C and 925 °C, it may be attributed to the release of He atoms from He-vacancy complexes with lower He/V ratio. For peaks located at more than 1000 °C, these He atoms dissociated from He bubbles may need higher energies and they should be attributed to the release of He atoms originating from He bubbles. Ultimately, the type of He atoms can be confirmed by the desorption activation energy corresponding to the desorption peak. The above results demonstrate that the RF magnetron sputtering can introduce different types of He atoms into the growing W films, and most of the introduced He atoms exist as He bubbles in deposited films.

3.3. TEM analysis

To observe the distribution and the size of He bubbles in W films, TEM observations of W films prepared in a mixture of gases with different He/Ar ratios were conducted. Fig. 6(a–c) shows the distribution of He bubbles in W films fabricated at different He/Ar ratios, and the mean diameter of these bubbles was estimated to be about 1.0 nm. As Fig. 6(a) shown, a large number of He bubbles distributed in the grain interiors and around the grain boundaries (GBs) of W films. In particular, the size of He bubbles trapped by GBs was bigger than that located in grain interiors. Moreover, these He bubbles around GBs were accumulated and connected to each other to form a necklace-like line as shown in Fig. 6(a). The above results indicate that the nucleation and growth of He bubbles are preferential on the GBs for rapid diffusion than that in the grain interiors, which had been found by J.H. Evans et al. and O. El-Atwani et al. [38,39]. This is because a large number of vacancies exist on the GBs so that more He atoms can be trapped by vacancies to form bubbles at GBs. Meanwhile, it was easily found that the shape of He bubbles in grain interiors was spherical and the shape of He bubbles trapped by the GBs was ellipsoidal. For this difference of He bubble shape, a similar phenomenon had been studied by A. Ofan et al. [40]. In their work, they believed that the shape of He bubbles is closely related to the surface free energy and the elastic free energy. As a result, in our experiments, when the surface energy was dominated, the spherical He bubbles in grain interiors were formed. When the elastic energy played a major role in this process, elongated He bubbles along the grain boundary were formed. For W films prepared at He/Ar = 2 and He/Ar = 3, He bubble size becomes a little larger than before, but the mean diameter of these bubbles was estimated to be still less than 2 nm, as shown in Fig. 6(b) and (c). At the same time, the concentration of He bubbles increased with the increase of He/Ar ratio. This is because with the increase of He/Ar ratio, more He atoms can be trapped into W films, which can contribute to forming more and bigger He bubbles. The result is also identical to the TDS profile shown in Fig. 5.

3.4. Hardness measurement

To investigate the effect of He/Ar ratio on the mechanical properties of W films, the hardness of W films was measured by nano-indentation. Fig. 7(a) shows that 4 indentation-depth curves of W films at RT and He/Ar = 0, 1, 2, 3. Considering that the thickness of tungsten films was about 5 μm (as shown in Fig. 4), to avoid the effect of surface roughness and substrate of thin film, the current nano-hardness values were determined by taking the average value at the indentation depth within the range of 10%–15% of the film thickness [41]. Therefore, nano-hardness of W films could be determined by averaging the values acquired from the stable region (400 nm–600nm) of the indentation profiles, as Fig. 7(a) shown.

The average nanoindentation hardness of W films fabricated at RT with different He/Ar ratios is shown in Fig. 7(b). As Fig. 7(b) shown, the hardness of W films at He/Ar = 0 is the smallest, as well as the hardness value increases significantly when He/Ar ratio is from 0 to 3. The increase of hardness value of W films may be positively related to the grain size and nano-sized He bubbles. However, combined with the results of Figs. 2 and 7(b), it was found that the hardness value of W films prepared at He/Ar = 3 was still much greater than that of W films prepared at He/Ar = 2 when the grain size hardly increased. The results indicate that the enhancement of the hardness of W films is mainly controlled by the effect of He bubbles. In terms of the hardening behaviors of He-charged W films, some W materials irradiated by He ions had also some similar phenomena [42–44]. These introduced nano-sized He bubbles (like dispersed particles) distributed in grain interiors and along the

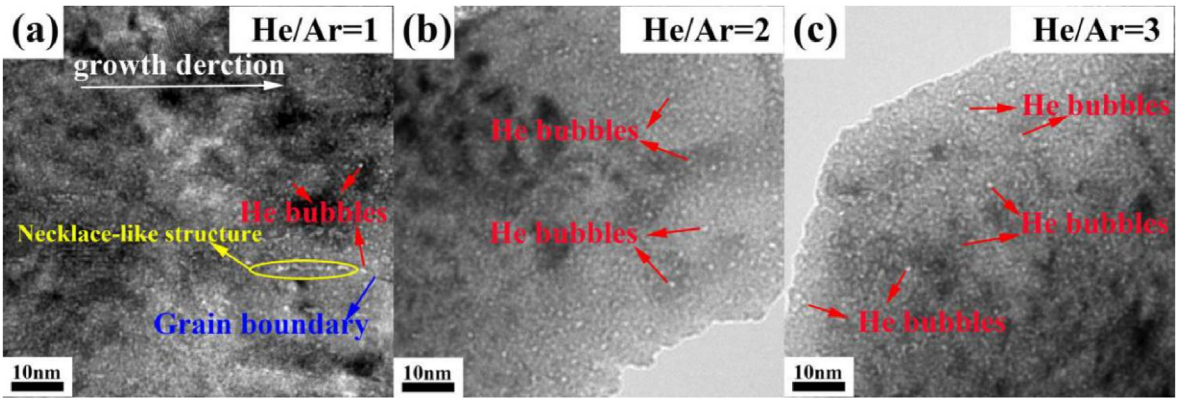

Fig. 6. TEM images of W films fabricated at different He/Ar ratios: (a) He/Ar = 1; (b) He/Ar = 2; (c) He/Ar = 3.

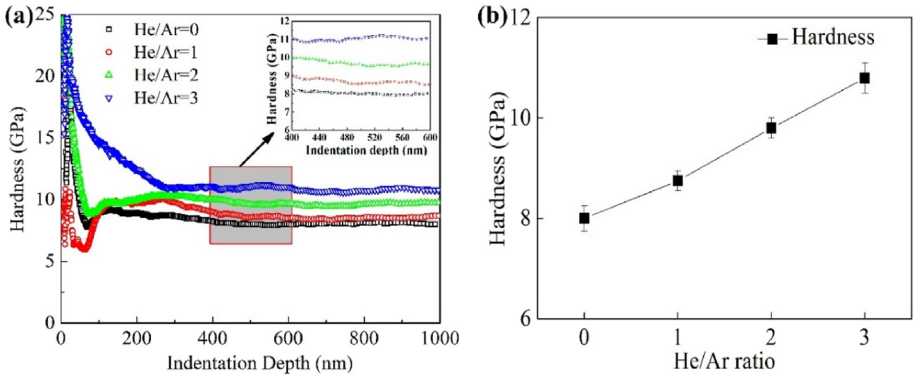

Fig. 7. The nano-hardness of W films with different He content: (a) Representative indentation-depth profiles of W films fabricated on Si substrates at RT under four He/Ar ratios of 0, 1:1, 2:1 and 3:1; (b) Average nanoindentation hardness value of W films in Fig. 7(a).

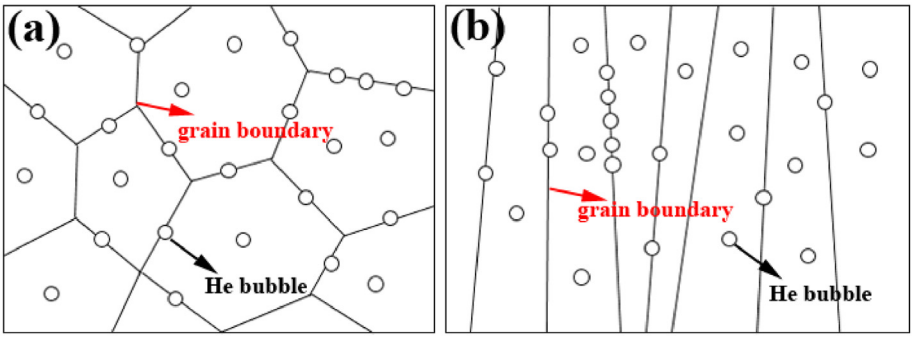

Fig. 8. The schematic diagram of the strengthening mechanism of He-charged W films: (a) Surface; (b) Cross-section.

grain boundaries, which may play the role of dispersion strengthening. The schematic diagram of the strengthening mechanism is shown in Fig. 8. It should be noted that the shape of He bubbles shown in Fig. 8 were assumed to be spherical to simplify the analysis, which couldn't reflect the actual shape of He bubbles. As Fig. 8 depicted, these nano-sized He bubbles can act as the barriers to dislocations motion, which results in the higher hardness of W films.

Generally, for He-charged materials, the change of hardness was associated with the number density and size of He bubbles [42,45]. In order to further analyze the relationship between the enhancement of hardness (ΔH) and He bubble, the Friedle-Kroupa-Hirsch (FKH) relation can be described as [46,47]:

$$\Delta\sigma = \frac{1}{8} MGbdN^{\frac{2}{3}} \tag{3}$$

where $\Delta\sigma$ is the strength change induced by bubbles, M is Taylor factor (3.06 for equiaxed BCC metals); G is the shear modulus (GPa); b is the Burgers vector (nm) of the dislocation; d is the bubble diameter (nm) and N is the bubble density (m^{-3}).

The increase in $\Delta\sigma$ from the FKH model corresponds to the increase of ΔH. Thus, for a given material containing He bubbles, the larger bubble size and/or bubble density, the higher the enhancement of hardness (ΔH). Therefore, compared with He-free W films,

the increment of the hardness of He-charged W film is due to the formation of He bubbles. For He-charged W films with different He content, the hardness value increased with He/Ar ratio increasing, which should be owing to the increase of He bubble size and density. Generally, the increment of hardness is actually no good to the characteristics of tungsten as a PFM. Because this can lead to an increase in the ductile-to-brittle transition temperature (DBTT), which is one of main causes of material failure under irradiation environment [48]. Thus, the inhibition of helium bubble nucleation and growth would be necessary. It can be tolerated by adding some dispersed nanoparticles and refining the grains of materials in nanometer size [49]. Relevant research will be carried out in subsequent experiments.

4. Conclusions

He-charged W films were prepared in a mixed atmosphere of He and Ar by RF magnetron sputtering. He concentration of W films can be controlled by adjusting He/Ar ration in a mixed atmosphere. XRD analysis and SEM images not only confirmed that the crystalline structure of deposited W films was in good accordance with that of the pure W target but also demonstrated that the deposited W films exhibited a typical columnar structure. TEM images showed that a large number of nano-sized He bubbles distributed in grain interiors and around the grain boundaries of W films, and the size of He bubbles in He-charged W films was about 1–2 nm. TDS analysis demonstrated that different kinds of He atoms can be introduced into W films, which include interstitial He atoms, He-vacancy complexes and He bubbles, etc. Nanoindentation measurements revealed that the hardness of W films increased with the He/Ar ratio increasing, which suggested that nano-sized He bubbles can strengthen W films.

Data availability

The raw/processed data required to reproduce these findings cannot be shared at this time due to legal or ethical reasons.

Declaration of competing interest

The authors declare that they have no known competing financial interests or personal relationships that could have appeared to influence the work reported in this paper.

CRediT authorship contribution statement

Le Wang: Conceptualization, Methodology, Funding acquisition, Writing - original draft. **Qunbo Fan:** Methodology, Visualization. **Ting Hao:** Methodology, Resources. **Duoduo Wang:** Investigation. **Xinjie Zhu:** Funding acquisition, Supervision, Writing - review & editing. **Haichao Gong:** Funding acquisition, Supervision, Writing - review & editing. **Xin Liu:** Funding acquisition, Supervision, Writing - review & editing.

Acknowledgments

This work was financially supported by the National Natural Science Foundation of China (Grant Nos.: 51571031; 11775255).

References

[1] G. Janeschitz, K. Borrass, G. Federici, Y. Igitkhanov, A. Kukushkin, H.D. Pacher, G.W. Pacher, M. Sugihara, The ITER divertor concept, J. Nucl. Mater. 220–222 (1995) 73–88.
[2] J.W. Davis, V.R. Barabash, A. Makhankov, L. Plöchl, K.T. Slattery, Assessment of tungsten for use in the ITER plasma facing components, J. Nucl. Mater. 258–263 (1998) 308–312.
[3] N. Yoshida, Review of recent works in development and evaluation of high-Z plasma facing materials, J. Nucl. Mater. 266–269 (1999) 197–206.
[4] H. Bolt, V. Barabash, W. Krauss, J. Linke, R. Neu, S. Suzuki, N. Yoshida, ASDEX Upgrade Team, Materials for the plasma-facing components of fusion reactors, J. Nucl. Mater. 329–333 (2004) 66–73.
[5] H. Iwakiri, K. Yasunaga, K. Morishita, N. Yoshida, Microstructure evolution in tungsten during low-energy helium ion irradiation, J. Nucl. Mater. 283–287 (2000) 1134–1138.
[6] R. Toschi, P. Barabaschi, D. Campbell, F. Elio, D. Maisonnier, D. Ward, How far is a fusion power reactor from an experimental reactor, Fusion Eng. Des. 56 (2001) 163–172.
[7] M.R. Gilbert, J.-Ch Sublet, Neutron-induced transmutation effects in W and W-alloys in a fusion environment, Nucl. Fusion 51 (2011), 043005.
[8] N.M. Ghoniem, M.L. Takata, A rate theory of swelling induced by helium and displacement damage in fusion reactor structural materials, J. Nucl. Mater. 105 (1982) 276–292.
[9] M.R. Gilbert, S.L. Dudarev, D. Nguyen-Manh, S. Zheng, L.W. Packer, J.-Ch Sublet, Neutron-induced dpa, transmutations, gas production, and helium embrittlement of fusion materials, J. Nucl. Mater. 442 (2013) S755–S760.
[10] B. Emmoth, Swelling of metallic surfaces irradiated by helium ions, Radiat. Eff. 78 (1983) 365–379.
[11] G. Was, Fundamentals of Radiation Materials Science, Springer-Verlag, Berlin, 2007.
[12] R. Niranjan, R.K. Rout, R. Srivastava, Y. Chakravarthy, P. Mishra, T.C. Kaushik, Satish, C. Gupta, Surface modifications of fusion reactor relevant materials on exposure to fusion grade plasma in plasma focus device, Appl. Surf. Sci. 355 (2015) 989–998.
[13] A.R. Kilmamentov, D.V. Gunderov, R.Z. Valiev, A.G. Balogh, H. Hahn, Enhanced ion irradiation resistance of bulk nanocrystalline TiNi alloy, Scripta Mater. 59 (2008) 1027–1030.
[14] N. Nita, R. Schaeublin, M. Victoria, Impact of irradiation on the microstructure of nanocrystalline materials, J. Nucl. Mater. 329–333 (2004) 953–957.
[15] H. Gleiter, Nanocrystalline materials, Prog. Mater. Sci. 33 (1989) 223–315.
[16] S. Wurstera, R. Pippan, Nanostructured metals under irradiation, Scripta Mater. 60 (2009) 1083–1087.
[17] W.J. Qin, F. Ren, R.P. Doerner, G. Wei, Y.W. L, S. Chang, M. Tang, H.Q. Deng, C.Z. Jiang, Y.Q. Wang, Nanochannel structures in W enhance radiation tolerance, Acta Mater. 153 (2018) 147–155.
[18] T. Tanno, A. Hasegawa, J.C. He, M. Fujiwara, S. Nogami, M. Satou, T. Shishido, K. Abe, Effects of transmutation elements on neutron irradiation hardening of tungsten, Mater. Trans. 48 (2007) 2399–2402.
[19] A. Hasegawa, T. Tanno, S. Nogami, M. Satou, Property change mechanism in tungsten under neutron irradiation in various reactors, J. Nucl. Mater. 417 (2011) 491–494.
[20] P.G. Raju, G. Michèle, Consequences of helium production from the radioactive decay of tritium on the properties of palladium tritide, Phys. Rev. B 66 (2002), 014105.
[21] G.J. Cheng, L.Q. Shi, X.S. Zhou, J.H. Liang, W.D. Wang, X.G. Long, B.F. Yang, S.M. Peng, Thermal desorption behavior of helium in aged titanium tritide films, J. Nucl. Mater. 466 (2015) 615–620.
[22] D.E.J. Armstrong, P.D. Edmondson, S.G. Roberts, Effects of sequential tungsten and helium ion implantation on nano-indentation hardness of tungsten, Appl. Phys. Lett. 102 (2013) 251901.
[23] S.J. Zenobia, L.M. Garrison, G.L. Kulcinski, The response of polycrystalline tungsten to 30 keV helium ion implantation at normal incidence and high temperatures, J. Nucl. Mater. 425 (2012) 83–92.
[24] A. Debelle, M. Barthe, T. Sauvage, R. Belamhawal, A. Chelgoum, P. Desgardin, H. Labrim, Helium behaviour and vacancy defect distribution in helium implanted tungsten, J. Nucl. Mater. 362 (2007) 181–188.
[25] S. Kajita, S. Takamura, N. Ohno, D. Nishijima, H. Iwakiri, N. Yoshida, Sub-ms laser pulse irradiation on tungsten target damaged by exposure to helium plasma, Nucl. Fusion 47 (2007) 1358–1366.
[26] S. Kajita, N. Ohno, M. Yajima, J. Kato, Growth annealing equilibrium of tungsten nanostructures by helium plasma irradiation in non-eroding regimes, J. Nucl. Mater. 440 (2013) 55–62.
[27] D.M. Mattox, G.J. Kominiak, Incorpation of helium in deposited gold films, J. Vac. Sci. Technol. 8 (1971) 194–198.
[28] H. Zheng, S. Liu, H.B. Yu, L.B. Wang, C.Z. Liu, L.Q. Shi, Introduction of helium into metals by magnetron sputtering deposition method, Mater. Lett. 59 (2005) 1071–1075.
[29] L.Q. Shi, C.Z. Liu, S. L Xu, Z.Y. Zhou, Helium-charged titanium films deposited by direct current magnetron sputtering, Thin Solid Films 479 (2005) 52–58.
[30] J.P. Jia, L.Q. Shi, X.C. Lai, Q.F. Wang, Preparation of Al thin films charged with helium by DC magnetron sputtering, Nucl. Instrum. Methods Phys. Res., Sect. B 263 (2007) 446–450.
[31] L. Song, X.P. Wang, F. Liu, Y.X. Gao, T. Zhang, G.N. Luo, Q.F. Fang, C.S. Liu, Microstructure and He desorption behaviors of He charged FeCrNi-based films fabricated by direct current magnetron sputtering, Thin Solid Films 589 (2015) 627–632.
[32] A.R. Krauss, D.M. Gruen, Determination of ion fraction and energy analysis of sputtered particles from deuterium bombarded surfaces, J. Nucl. Mater. 63 (1976) 380–385.
[33] L. Wang, T. Hao, B.L. Zhao, T. Zhang, Q.F. Fang, C.S. Liu, X.P. Wang, L. Cao, Evolution behavior of helium bubbles and thermal desorption study in

helium-charged tungsten film, J. Nucl. Mater. 508 (2018) 107–115.
[34] B.D. Cullity, Elements of X-Ray Diffraction, Addison-Wesley Publishing Company Inc., California, 1956.
[35] G.K. Williamson, W.H. Hall, X-ray line broadening from filed aluminum and wolfram, Acta Metall. 1 (1953) 22–31.
[36] W.J. Qin, F. Ren, J. Zhang, X.N. Dong, Y.J. Feng, H. Wang, J. Tang, G.X. Cai, Y.Q. Wang, C.Z. Jiang, Helium retention in krypton ion pre-irradiated nanochannel W film, Nucl. Fusion 58 (2018), 026021.
[37] C.S. Becquart, C. Domain, An object kinetic Monte Carlo simulation of the dynamics of helium and point defects in tungsten, J. Nucl. Mater. 385 (2009) 223–227.
[38] J.H. Evans, A. van Veen, J.T.M. de Hosson, R. Bullough, J.R. Willis, The trapping of helium at a low angle tilt boundary in molybdenum, J. Nucl. Mater. 125 (1984) 298.
[39] O. El-Atwani, K. Hattar, J.A. Hinks, G. Greaves, S.S. Harilal, A. Hassanein, Helium bubble formation in ultrafine and nanocrystalline tungsten under different extreme conditions, J. Nucl. Mater. 458 (2015) 216–223.
[40] A. Ofan, L.H. Zhang, O. Gaathon, S. Bakhru, H. Bakhru, Y.M. Zhu, D. Welch, R.M. Osgood Jr., Spherical solid He nanometer bubbles in an anisotropic complex oxide, Phys. Rev. B 82 (2010) 104113.
[41] I.-L. Velicu, V. Tiron, C. Porosnicu, I. Burducea, N. Lupu, G. Stoian, G. Popa, D. Munteanu, Enhanced properties of tungsten thin films deposited with a novel HiPIMS approach, Appl. Surf. Sci. 424 (2017) 397–406.
[42] M.H. Cui, T.L. Shen, L.L. Pang, Y.B. Zhu, P. Jin, C. Liu, X.S. Fang, Z.G. Wang, He ion implantation induced He bubbles and hardness in tungsten, Nucl. Mater. Energy 15 (2018) 232–236.
[43] M.Z. Zhao, F. Liu, Z.S. Yang, Q. Xu, F. Ding, X.C. Li, H.S. Zhou, G.N. Luo, Fluence dependence of helium ion irradiation effects on the microstructure and mechanical properties of tungsten, Methods Phys. Res., Sect. B 414 (2018) 121–125.
[44] W.J. Qin, Y.Q. Wang, M. Tang, F. Ren, Q. Fu, G.X. Cai, L. Dong, L.L. Hu, G. Wei, C.Z. Jiang, Microstructure and hardness evolution of nanochannel W films irradiated by helium at high temperature, J. Nucl. Mater. 502 (2018) 132–140.
[45] F.H. Kong, M. Qu, S. Yan, A.L. Zhang, S.X. Peng, J.M. Xue, Y.G. Wang, Helium induced hardening effect in polycrystalline tungsten, Nucl. Instrum. Methods B 406 (2017) 643–647.
[46] J. Friedel, CXXX. On the linear work hardening mate of face-centred cubic single crystals, the London, Edinb, Dublin Philos. Mag. J. Sci. 46 (1955) 1169–1186.
[47] F. Kroupa, P.B. Hirsch, Elastic interaction between prismatic dislocation loops and straight dislocations, Discuss. Faraday Soc. 38 (1964) 49–55.
[48] V. Barabash, G. Federici, M. Rödig, L.L. Snead, C.H. Wu, Neutron irradiation effects on plasma facing materials, J. Nucl. Mater. 283–287 (2000) 138–146.
[49] G.M. Cheng, W.Z. Xu, Y.Q. Wang, A. Misra, Y.T. Zhu, Grain size effect on radiation tolerance of nanocrystalline Mo, Scripta Mater. 123 (2016) 90–94.